OPEN ACCESS

ISAR Journal of Science and Technology

Volume 3, Issue 6, 2025, Page: 5-19

Abbriviate Title- ISAR J Sci Tech

ISSN *(Online)*- 2584-2056

https://isarpublisher.com/journal/isarjst

EFFECTS OF VARIATION IN SOOT AEROSOL CONCENTRATIONS AND RELATIVE HUMIDITY IMPACT ON THE POLARIZABILITY AND PHASE FUNCTION OF URBAN ATMOSPHERE

A. Aliyu[1*], F. Shuaibu[2], B. I. Tijjani[3] and U. M. Gana[3]

[1] Department of Physics, Aliko Dangote University of Science and Technology Wudil, Kano State, Nigeria.

[2] Department of Physics, RMK, C.A.R.S, Tudun Wada, Kano State, Nigeria.

[3] Department of Physics, Bayero University Kano, Kano State, Nigeria.

***Corresponding Author**

Aliyu Aliyu

Department of Physics, Aliko Dangote University of Science and Technology Wudil, Kano State, Nigeria.

Article History

Received: 07.04.2025
Accepted: 18.05.2025
Published: 09.06.2025

Abstract: This study investigates the impact of varying soot aerosol concentrations and relative humidity (RH) on the polarizability and phase function of non-spherical urban atmospheric aerosols. Using the Optical Properties of Aerosols and Clouds (OPAC 4.0) software, urban aerosol optical properties at visible wavelengths (0.4 - 0.8 μm) were simulated across eight relative humidities (0%, 50%, 70%, 80%, 90%, 95%, 98%, 99%). The Stokes parameters are employed to derive phase functions, while the Claussi-Massoti formulation, combined with Maxwell and Lorentz-Lorentz relations, were used for computation of effective polarizabilities. The results provide insights into RH and soot aerosol concentration effects on urban aerosol optical properties, including effective polarizabilities, polarization, and phase function data. The extraction of these data using OPAC 4.0 and determination of aerosol size growth curves' mean exponent through effective hygroscopic growth. Effective polarizability exhibits a decrease with increasing wavelength and soot aerosols concentration, whereas it increases with increasing relative humidity.

Keywords: aerosols, polarization, polarizability, and phase function.

Cite this article:

Aliyu, A., Shuaibu, F., Tijjani, B. I., and Gana, U. M., (2025). EFFECTS OF VARIATION IN SOOT AEROSOL CONCENTRATIONS AND RELATIVE HUMIDITY IMPACT ON THE POLARIZABILITY AND PHASE FUNCTION OF URBAN ATMOSPHERE. *ISAR Journal of Science and Technology*, *3*(6), 5-19.

1 INTRODUCTION

Urban air pollution is a pressing concern due to the diverse range of aerosols emitted into the atmosphere. The intricate shapes and structures of these aerosols dictate their optical properties, which are vital for understanding their effects on climate, visibility, and public health. Aerosol particles have the ability to polarize light, known as polarizability (Mishchenko *et al*., 2002), which is influenced by factors like size, shape, and composition. The phase function describes the scattering of light by aerosols in various directions, providing crucial data for radiative transfer calculations and remote sensing applications. Despite ongoing research, quantifying the impact of aerosols on the atmospheric energy budget remains a significant challenge (Anderson *et al*., 2003). The lack of accurate methods for identifying and characterizing aerosols hinders our understanding of their physical properties (Anderson *et al*., 2003; Schwartz and Andreae, 1996). To bridge this knowledge gap, researchers have developed various methods and models, including OPAC 4.0, (Koepke *et al*., 2015) which utilizes Mie theory to simulate aerosol optical properties (Hess, Koepke, and Schult, 1998). OPAC takes into account factors like shape, refractive index, size distribution, and composition to accurately calculate polarizability and phase function.

Previous studies have explored the optical properties of aerosols, including polarizability and phase function (Smith and Johnson, 2010; Mishchenko *et al*., 2002). This study seeks to expand on existing knowledge by employing OPAC to investigate the polarizability and phase function of urban non-spherical aerosols. The findings will offer valuable insights into the scattering patterns and polarization behavior of these aerosols, ultimately enhancing our understanding of their impact on urban air quality and climate.

This is an open access article under the CC BY-NC license

2 METHODOLOGY

The approach to be employed for analysing the OPAC 4.0 dataset to fulfil the research objectives is outlined.

2.1 OPAC 4.0

The OPAC software package, developed by Hess *et al*. (1998), is a vital tool for climate modelers, providing comprehensive datasets on atmospheric aerosol optical properties. OPAC's intuitive interface and FORTRAN program enable efficient computation of optical properties for various cloud and aerosol combinations, streamlining the modelling workflow. Urban aerosol model variants are derived from OPAC 4.0 across eight relative humidity levels (0%, 50%, 70%, 80%, 90%, 95%, 98%, 99%) and wavelengths spanning 0.25-40 micrometres. Urban aerosols consist of three components: water-soluble, insoluble, and soot. OPAC 4.0 combines these components to generate aerosol types.

This study systematically varies soot aerosol component concentrations in incremental increments, keeping water-soluble and insoluble components constant. Five models were developed, each with increasing soot component concentrations (30% relative to the base model). Using the OPAC FORTRAN program, the study computes optical properties for each model, including extinction coefficient, scattering coefficient, absorption coefficient, single scattering albedo, and asymmetric parameters. These properties are obtained at all relative humidity levels and spectral wavelengths (0.4-0.8 µm).

The models extracted from OPAC 4.0 are given below in table 1

Table 1 the microphysical properties of the urban aerosols at 0% RH (Hess *et al*, 1998).

Components	R_{min} (µm)	R_{max} (µm)	Sigma	R_{dry} (µm)
Waso	0.005	20.00	2.24	0.0212
Inso	0.005	20.00	2.51	0.4710
Soot	0.005	20.00	2.00	0.0118

Table 2: Five Model Component Mixtures with Varying SOOT Aerosol Concentrations

	Model 1	Model 2	Model 3	Model 4	Model 5
Components	No. Den(cm^{-3})	No. Den(cm^{-3})	No. Den(cm^{-3})	No. Den(cm^{-3})	No. Den(cm^{-3})
INSO	1.50	1.50	1.50	1.50	1.50
WASO	28,000.00	28,000.00	28,000.00	28,000.00	28,000.00
SOOT	**130,000.00**	**169,000.00**	**208,000.00**	**247,000.00**	**286,000.00**

Table 2 describes the urban aerosols simulated with varying soot (non-spherical) component. The number concentrations were increased by adding 30% of model 1 model to subsequent models.

2.2 Polarizability

From Shettle and Fenn, (1979), the well-known Lorentz - Lorentz relation between the refractive index n and polarizability α is given as

$$\alpha = \frac{3(n^2-1)}{\rho(n^2+2)} \quad (1)$$

when the material has absorbing properties the refractive index is expressed as complex number $n = n' + ik$, where n is the complex refractive index of the material, n' is the real part of the refractive index, representing the material's ability to bend light (also known as the refractive index in non-absorbing materials), i is the imaginary unit, which satisfies $i^2 = -1$, k the imaginary part of the refractive index, representing the material's ability to absorb light (also known as the extinction coefficient), and ρ is the number density. Equation (1) gives the polarizability of one type of aerosol.

To determine the effective polarizability of the mixture the following addition relation is used.

$$\alpha_{eff} = \sum_{i=1}^{n} V_i \alpha_i \quad (2)$$

where α_{eff} is the effective polarizability of the mixtures, V_i is the volume mix ratio of the i^{th} aerosol component, α_i is the polarizability of the i^{th} component.

2.3 Phase functions

The function $F_{11}(\Theta)$ is called the phase function and is normalized to 1 such that (Lindqvist *et al.*, 2014),

$$\frac{1}{2}\int_0^{\pi} \sin(\Theta) F_{11}(\Theta) d\Theta = 1 \quad (3)$$

where Θ is the scattering angle, $F_{11}(\Theta)$ is proportional to the scattered intensity as a function of the scattering angle. It describes the angular distribution of the scattered light by aerosols, and provides information about the relative intensity and directionality of scattered light at different scattering angles.

3. RESULTS AND DISCUSSIONS

The graphs of phase function with scattering angles and effective polarizabilities with wavelengths (0.4 to 0.8 µm) at eight relative humidities are presented. The graphs are presented as figures (a) and figures (b). The figures (a) displays the phase function plots from 0 to 180 degrees. However, due to the dense packing of the plots, Figure (b) is used to illustrate the effect of forward scattering angles on the phase functions.

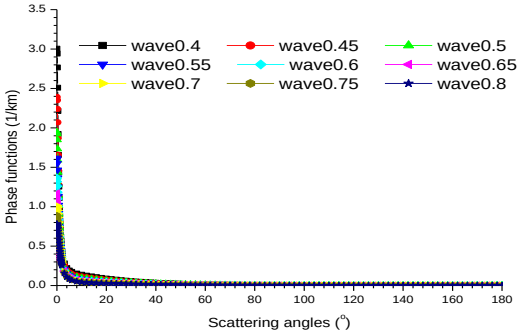

Figure 1(a): A graph of Phase functions against scattering angles at 0% RH SOOT Model 1

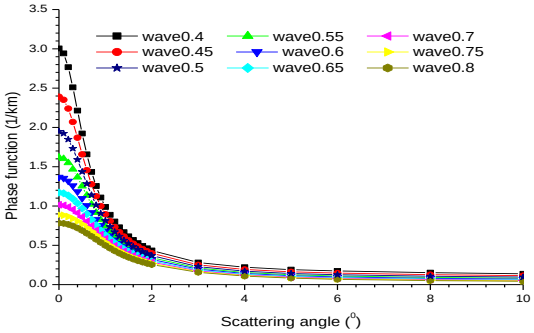

Figure 1(b): A graph of Phase functions against scattering angles at 0% RH SOOT Model 1

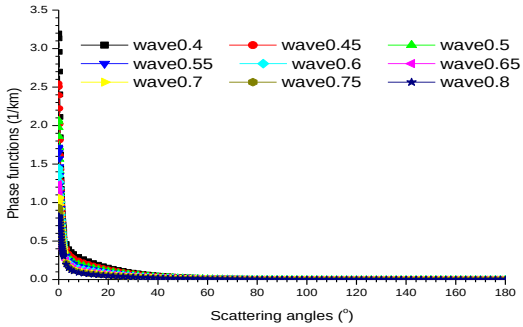

Figure 2(a): A graph of Phase functions against scattering angles at 50% RH SOOT Model 1

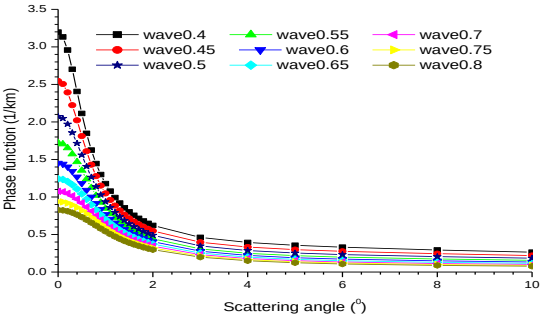

Figure 2(b): A graph of Phase functions against scattering angles at 50% RH SOOT Model 1

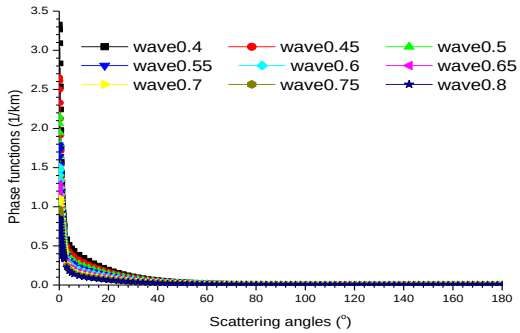

Figure 3(a): A graph of Phase functions against scattering angles at 70% RH SOOT Model 1

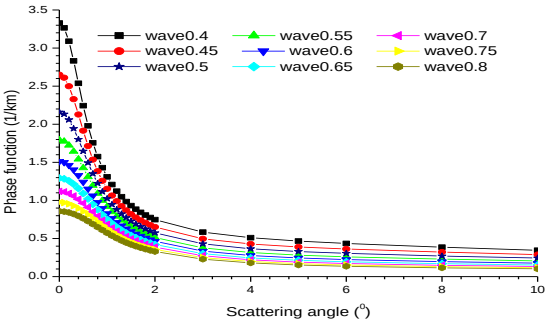

Figure 3(b): A graph of Phase functions against scattering angles at 70% RH SOOT Model 1

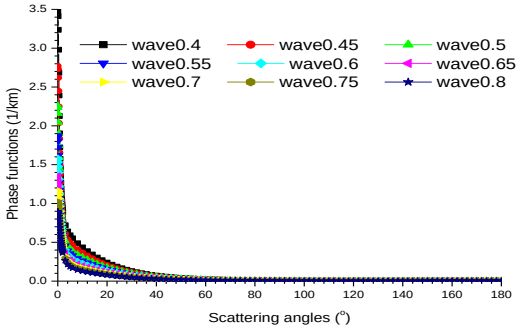

Figure 4(a): A graph of Phase functions against scattering angles at 80% RH SOOT Model 1

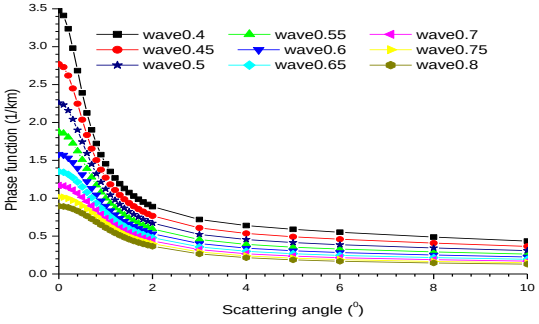

Figure 4(b): A graph of Phase functions against scattering angles at 80% RH SOOT Model 1

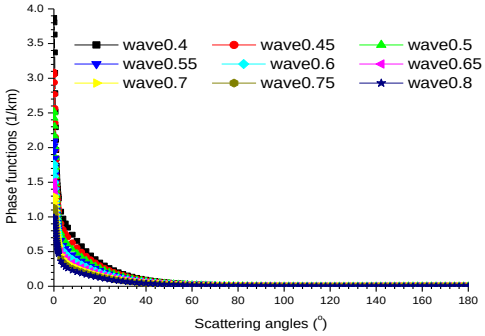

Figure 5(a): A graph of Phase functions against scattering angles at 90% RH SOOT Model 1

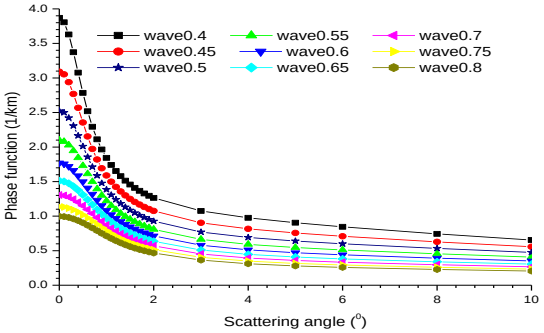

Figure 5(b): A graph of Phase functions against scattering angles at 90% RH SOOT Model 1

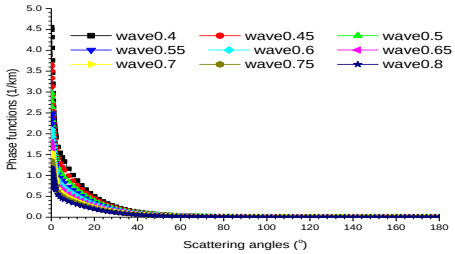

Figure 6(a): A graph of Phase functions against scattering angles at 95% RH SOOT Model 1

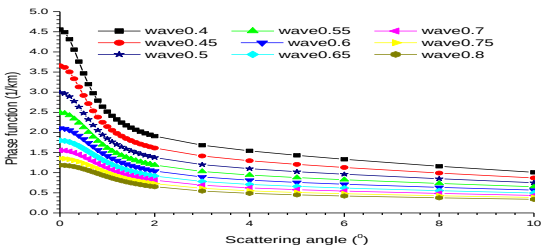

Figure 6(b): A graph of Phase functions against scattering angles at 95% RH SOOT Model 1

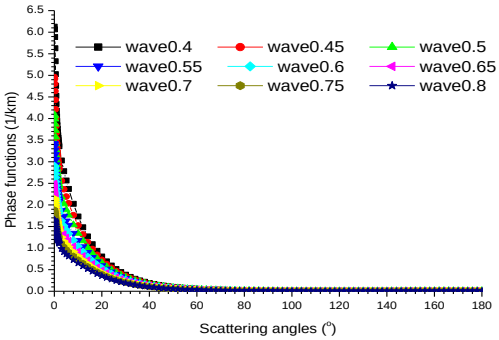

Figure 7(a): A graph of Phase functions against scattering angles at 98% RH SOOT Model 1

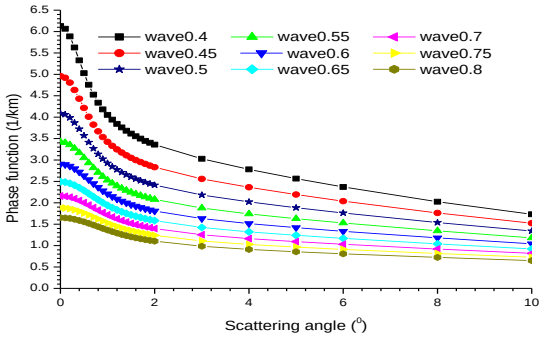

Figure 7(b): A graph of Phase functions against scattering angles at 98% RH SOOT Model 1

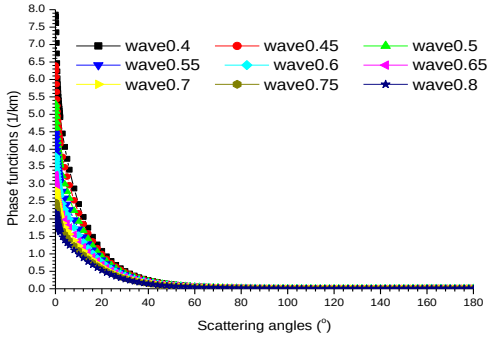

Figure 8(a): A graph of Phase functions against scattering angles at 99% RH SOOT Model 1

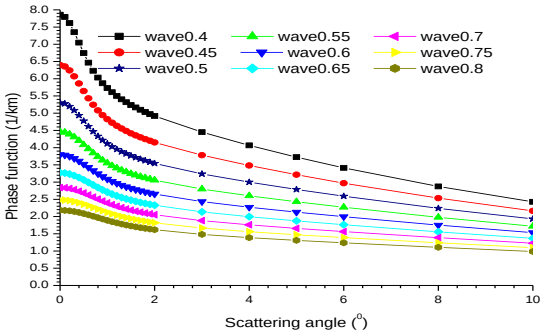

Figure 8(b): A graph of Phase functions against scattering angles at 99% RH SOOT Model 1

Figures 1-8 demonstrate that the phase functions decrease with increasing scattering angles and demonstrated high aerosol concentrations in urban areas, leading to increased scattering and a decrease in phase functions with increasing scattering angle because the phase functions are more pronounced at lower scattering angles. When all the plots were compared, it is evident that the phase functions increase with increasing relative humidity due to the aerosols growth cause by water uptake, which enhances their scattering properties, resulting in an increase in phase function. The phase functions decrease with increasing wavelength due to decrease in scattering with increasing wavelength, leading to a decrease in phase functions, as can be clearly seen from figures 1b to 8b.

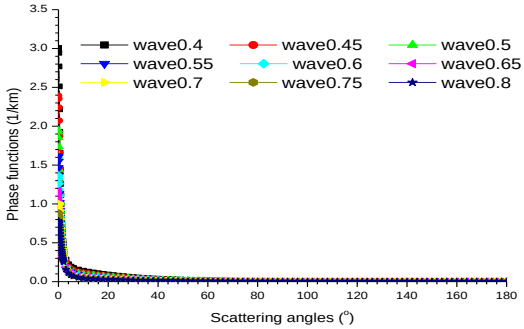

Figure 9(a): A graph of Phase functions against scattering angles at 0% RH SOOT Model 2

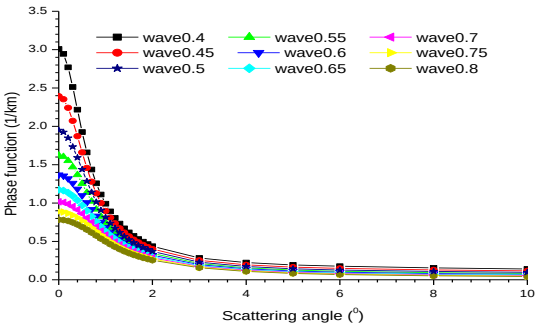

Figure 9(b): A graph of Phase functions against scattering angles at 0% RH SOOT Model 2

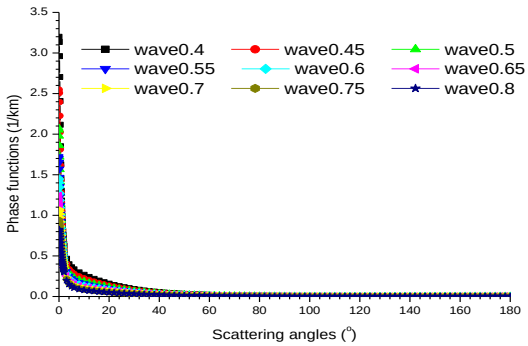

Figure 10(a): A graph of Phase functions against scattering angles at 50% RH SOOT Model 2

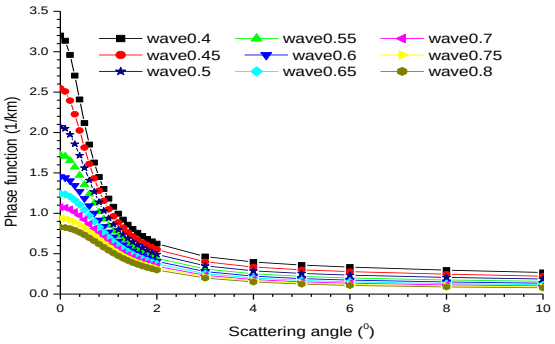

Figure 10(b): A graph of Phase functions against scattering angles at 50% RH SOOT Model 2

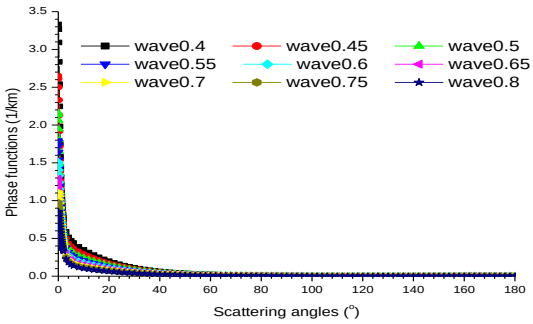

Figure 11(a): A graph of Phase functions against scattering angles at 70% RH SOOT Model 2

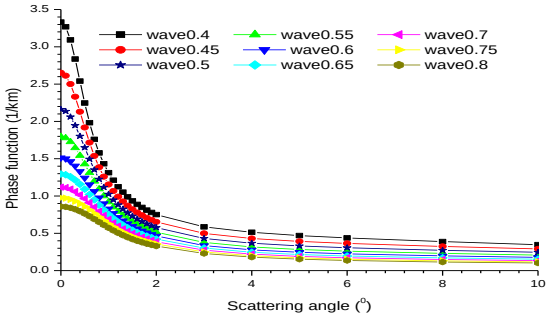

Figure 11(b): A graph of Phase functions against scattering angles at 70% RH SOOT Model 2

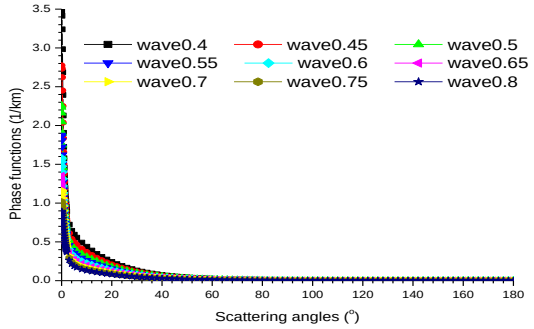

Figure 12(a): A graph of Phase functions against scattering angles at 80% RH SOOT Model 2

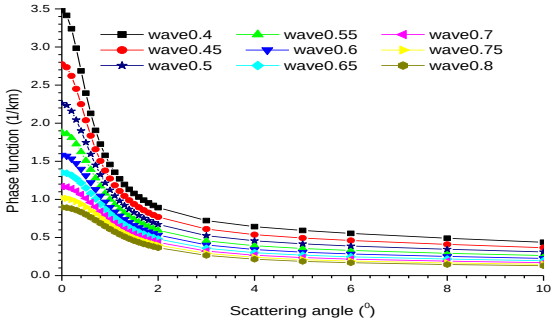

Figure 12(b): A graph of Phase functions against scattering angles at 80% RH SOOT Model 2

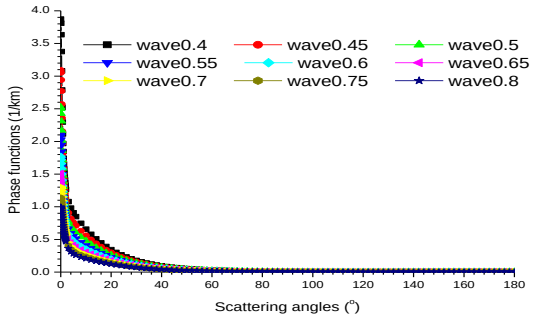

Figure 13(a): A graph of Phase functions against scattering angles at 90% RH SOOT Model 2

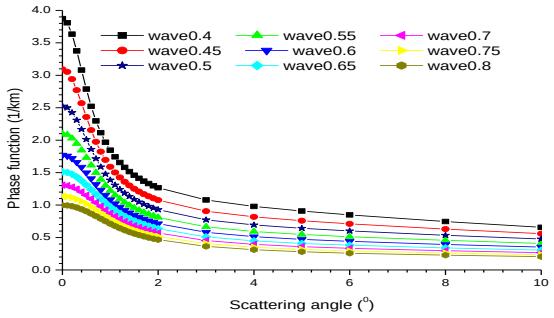

Figure 13(b): A graph of Phase functions against scattering angles at 90% RH SOOT Model 2

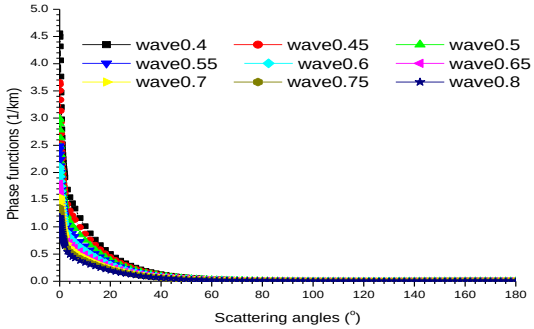

Figure 14(a): A graph of Phase functions against scattering angles at 95% RH SOOT Model 2

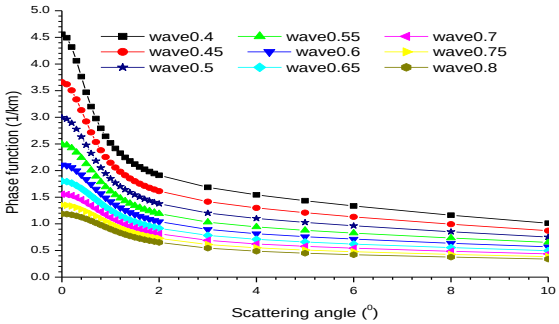

Figure 14(b): A graph of Phase functions against scattering angles at 95% RH SOOT Model 2

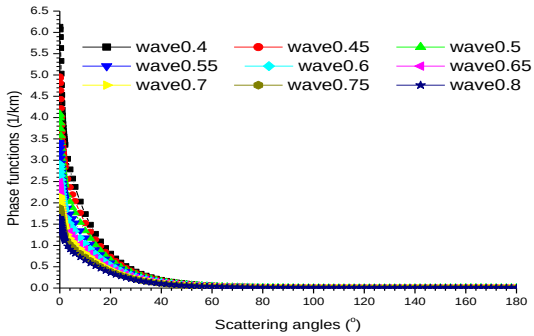

Figure 15(a): A graph of Phase functions against scattering angles at 98% RH SOOT Model 2

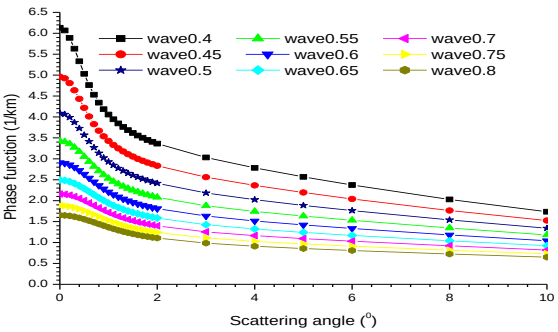

Figure 15(b): A graph of Phase functions against scattering angles at 98% RH SOOT Model 2

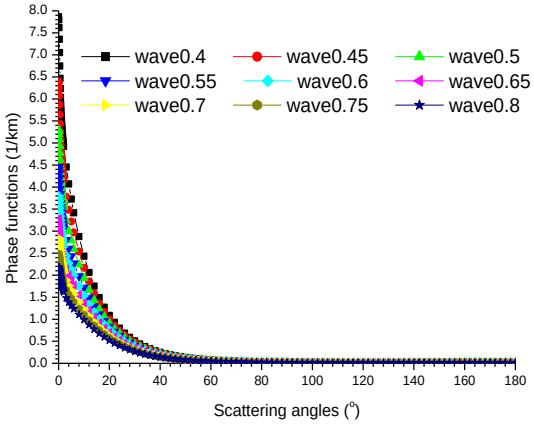

Figure 16(a): A graph of Phase functions against scattering angles at 99% RH SOOT Model 2

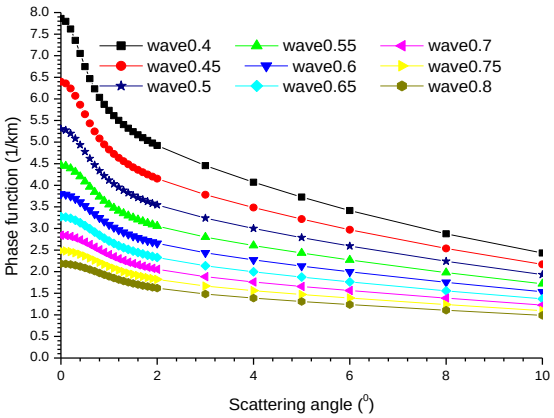

Figure 16(b): A graph of Phase functions against scattering angles at 99% RH SOOT Model 2

The results show that phase functions decrease with increasing scattering angles, consistent with the dominance of forward scattering at lower angles. This trend is particularly notable in urban areas with high aerosol concentrations. Phase functions increase with increasing relative humidity due to aerosol growth from water uptake, which enhances scattering properties. However, phase functions decrease with increasing wavelength, reflecting reduced scattering efficiency as can be clearly seen from figures 9b-16b.

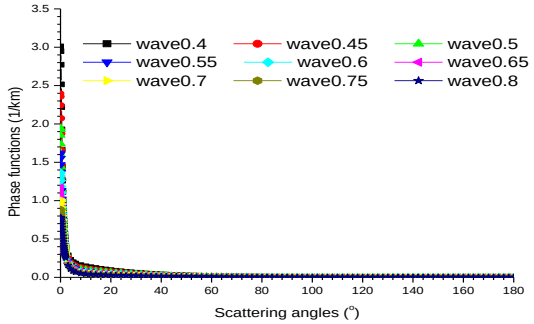

Figure 17(a): A graph of Phase functions against scattering angles at 0% RH SOOT Model 3

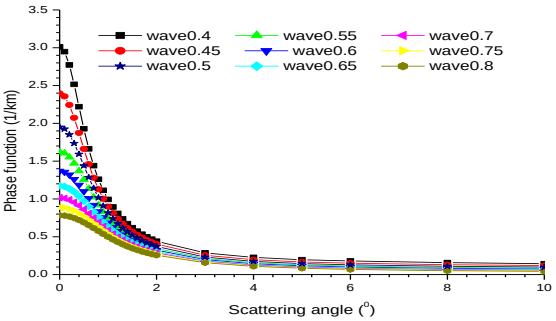

Figure 17(b): A graph of Phase functions against scattering angles at 0% RH SOOT Model 3

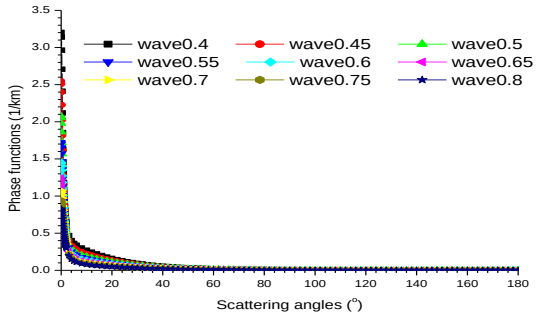

Figure 18(a): A graph of Phase functions against scattering angles at 50% RH SOOT Model 3

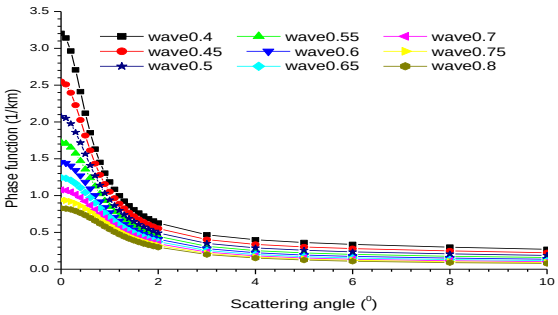

Figure 18(b): A graph of Phase functions against scattering angles at 50% RH SOOT Model 3

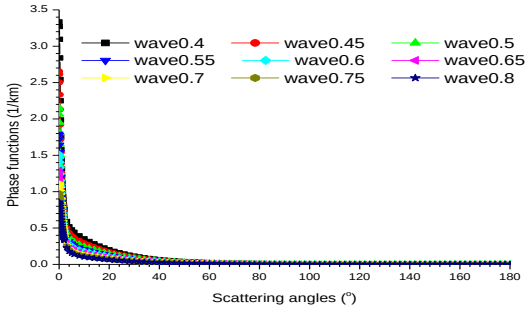

Figure 19(a): A graph of Phase functions against scattering angles at 70% RH SOOT Model 3

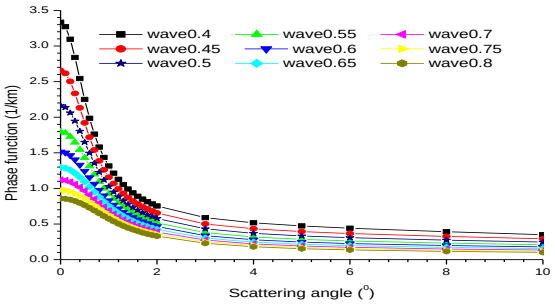

Figure 19(b): A graph of Phase functions against scattering angles at 70% RH SOOT Model 3

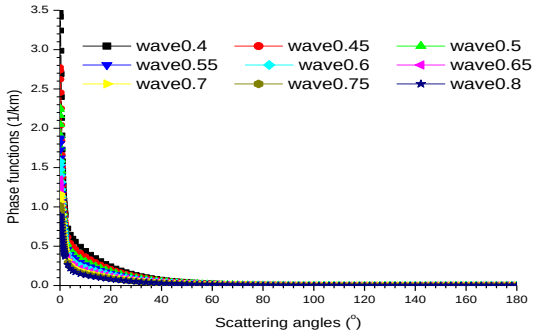

Figure 20(a): A graph of Phase functions against scattering angles at 80% RH SOOT Model 3

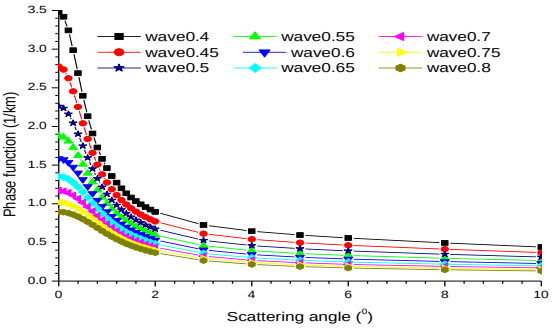

Figure 20(b): A graph of Phase functions against scattering angles at 80% RH SOOT Model 3

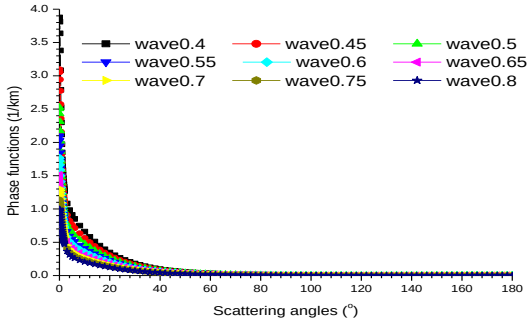

Figure 21(a): A graph of Phase functions against scattering angles at 90% RH SOOT Model 3

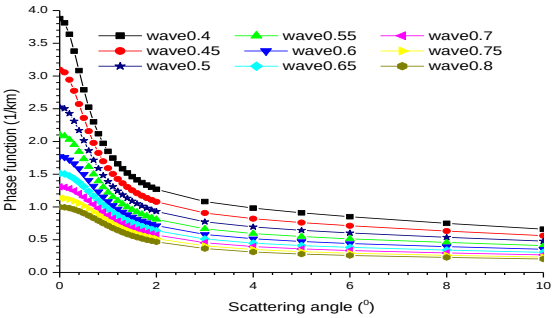

Figure 21(b): A graph of Phase functions against scattering angles at 90% RH SOOT Model 3

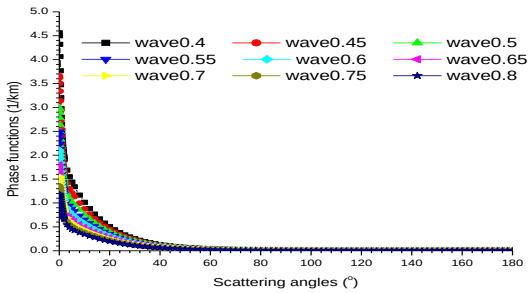

Figure 22(a): A graph of Phase functions against scattering angles at 95% RH SOOT Model 3

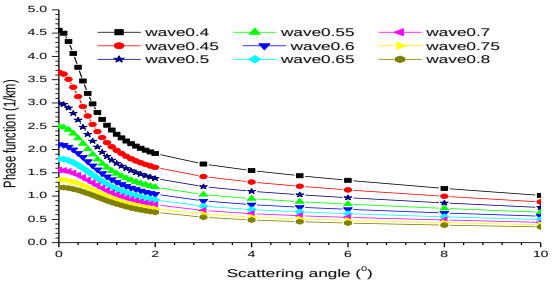

Figure 22(b): A graph of Phase functions against scattering angles at 95% RH SOOT Model 3

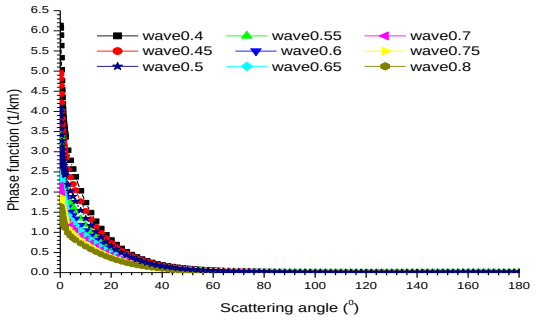

Figure 23(a): A graph of Phase functions against scattering angles at 98% RH SOOT Model 3

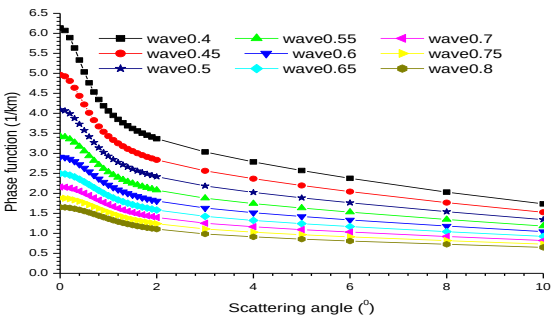

Figure 23(b): A graph of Phase functions against scattering angles at 98% RH SOOT Model 3

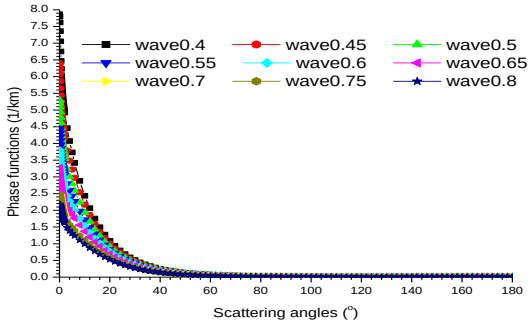

Figure 24(a): A graph of Phase functions against scattering angles at 99% RH SOOT Model 3

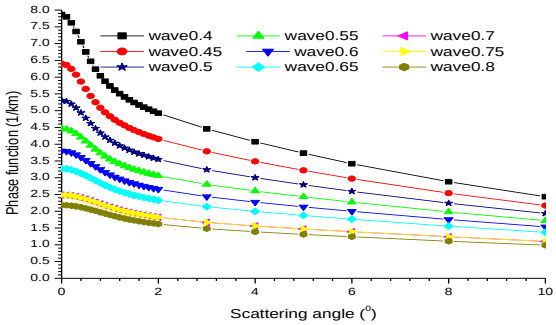

Figure 24(b): A graph of Phase functions against scattering angles at 99% RH SOOT Model 3

The phase functions decrease with increasing scattering angles, particularly in urban areas with high aerosol concentrations, where forward scattering dominates at lower angles. Conversely, phase functions increase with increasing relative humidity due to aerosol growth from water uptake, which enhances scattering properties. However, phase functions decrease with increasing wavelength, reflecting reduced scattering efficiency. These trends are consistently observed across the figures 17b-24b.

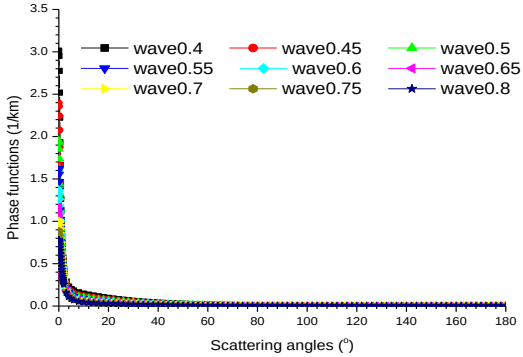

Figure 25(a): A graph of Phase functions against scattering angles at 0% RH SOOT Model 4

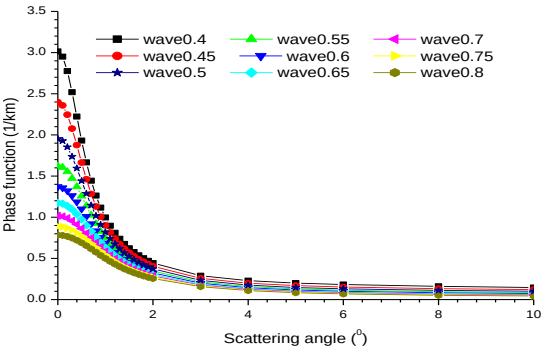

Figure 25(b): A graph of Phase functions against scattering angles at 0% RH SOOT Model 4

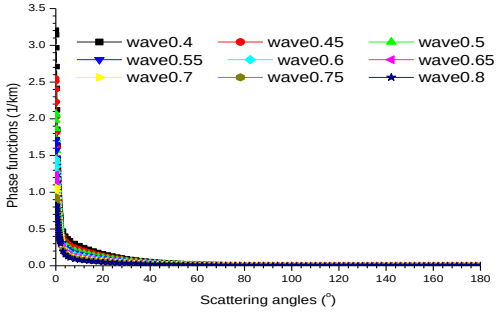

Figure 26(a): A graph of Phase functions against scattering angles at 50% RH SOOT Model 4

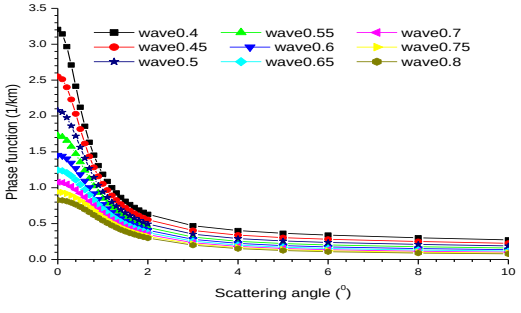

Figure 26(b): A graph of Phase functions against scattering angles at 50% RH SOOT Model 4

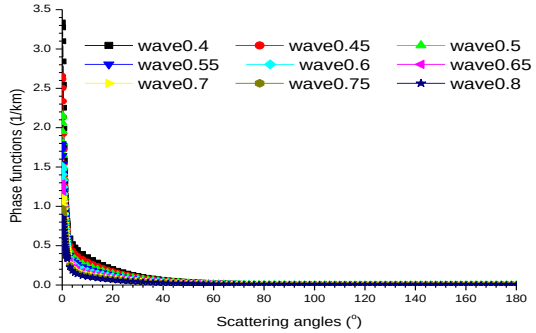

Figure 27(a): A graph of Phase functions against scattering angles at 70% RH SOOT Model 4

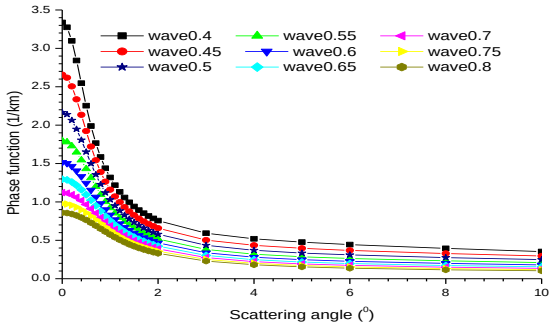

Figure 27(b): A graph of Phase functions against scattering angles at 70% RH SOOT Model 4

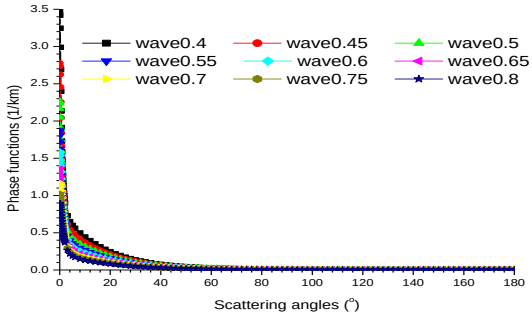

Figure 28(a): A graph of Phase functions against scattering angles at 80% RH SOOT Model 4

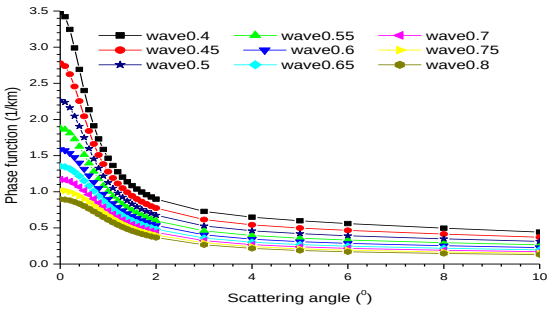

Figure 28(b): A graph of Phase functions against scattering angles at 80% RH SOOT Model 4

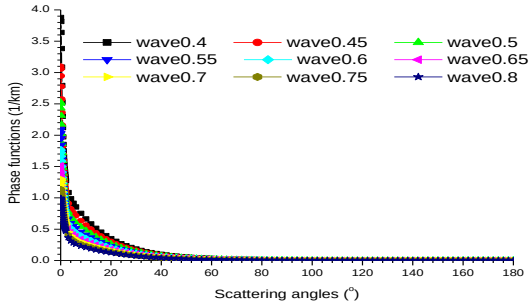

Figure 29(a): A graph of Phase functions against scattering angles at 90% RH SOOT Model 4

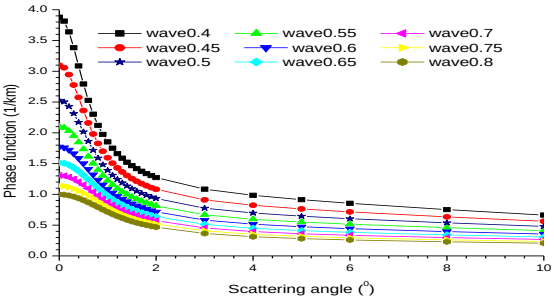

Figure 29(b): A graph of Phase functions against scattering angles at 90% RH SOOT Model 4

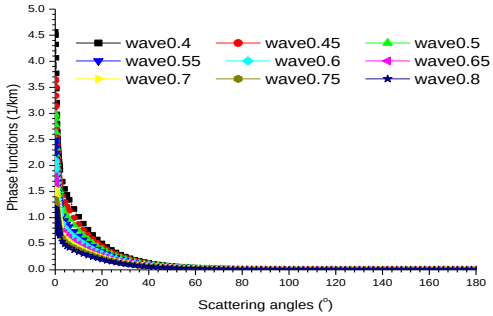

Figure 30(a): A graph of Phase functions against scattering angles at 95% RH SOOT Model 4

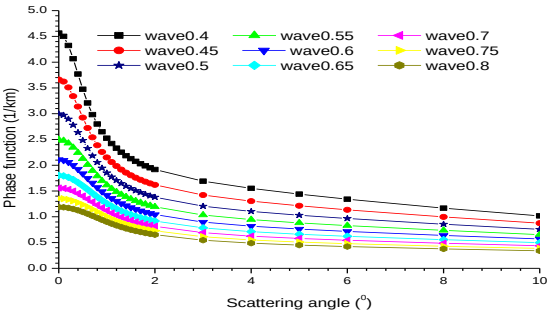

Figure 30(b): A graph of Phase functions against scattering angles at 95% RH SOOT Model 4

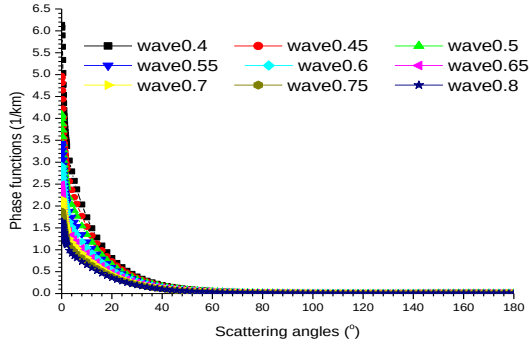

Figure 31(a): A graph of Phase functions against scattering angles at 98% RH SOOT Model 4

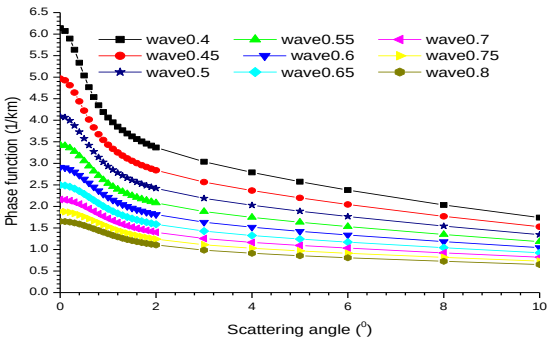

Figure 31(b): A graph of Phase functions against scattering angles at 98% RH SOOT Model 4

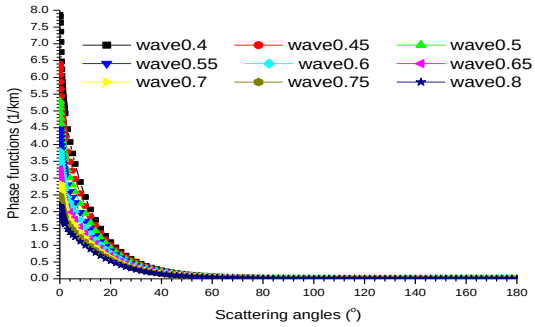

Figure 32(a): A graph of Phase functions against scattering angles at 99% RH SOOT Model

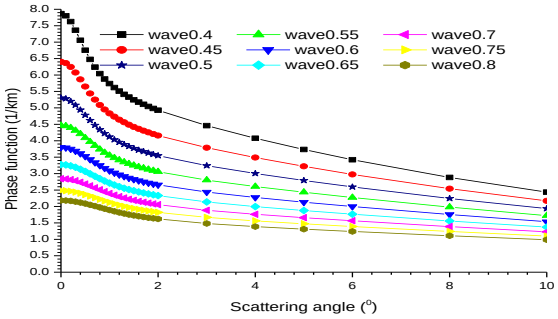

Figure 32(b): A graph of Phase functions against scattering angles at 99% RH SOOT Model 4

The results show that phase functions decrease with increasing scattering angles, particularly in urban areas with high aerosol concentrations, where forward scattering is more pronounced at lower angles. Phase functions increase with increasing relative humidity due to aerosol growth and enhanced scattering properties. However, as wavelength increases, phase functions decrease due to reduced scattering efficiency. These trends are consistently observed across the figures 25b-32b.

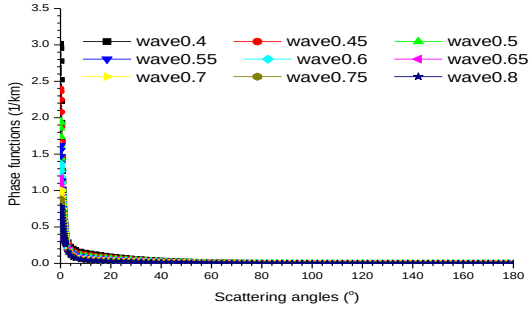

Figure 33(a): A graph of Phase functions against scattering angles at 0% RH SOOT Model 5

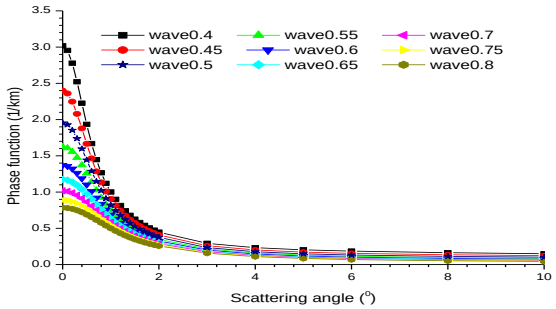

Figure 33(b): A graph of Phase functions against scattering angles at 0% RH SOOT Model 5

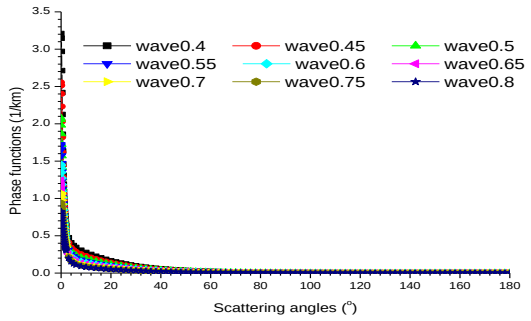

Figure 34(a): A graph of Phase functions against scattering angles at 50% RH SOOT Model 5

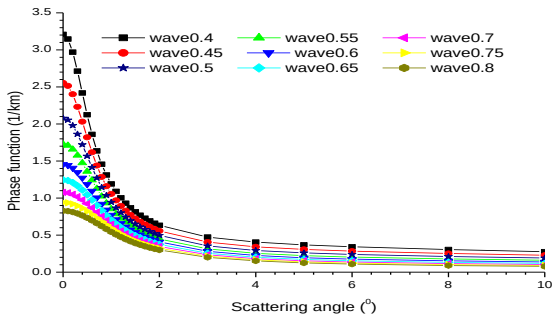

Figure 34(b): A graph of Phase functions against scattering angles at 50% RH SOOT Model 5

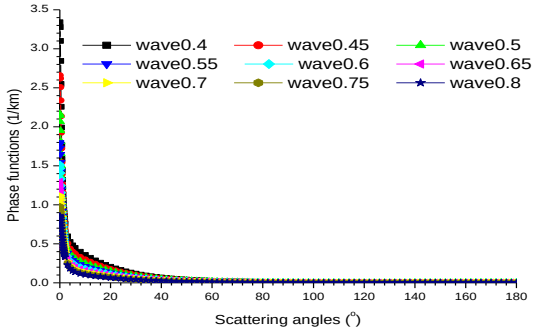

Figure 35(a): A graph of Phase functions against scattering angles at 70% RH SOOT Model 5

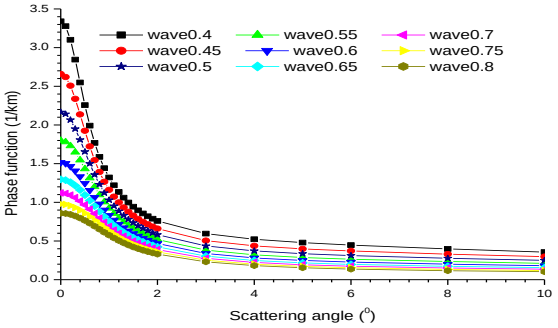

Figure 35(b): A graph of Phase functions against scattering angles at 70% RH SOOT Model 5

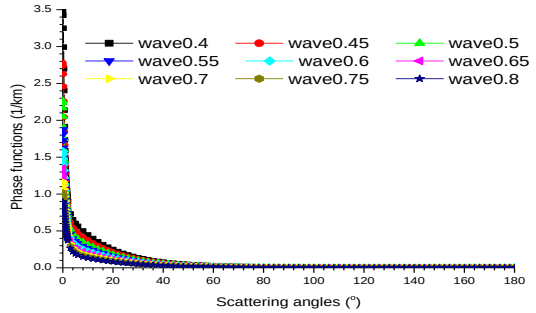

Figure 36(a): A graph of Phase functions against scattering angles at 80% RH SOOT Model 5

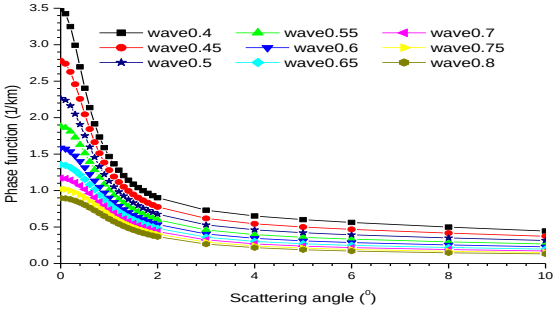

Figure 36(b): A graph of Phase functions against scattering angles at 80% RH SOOT Model 5

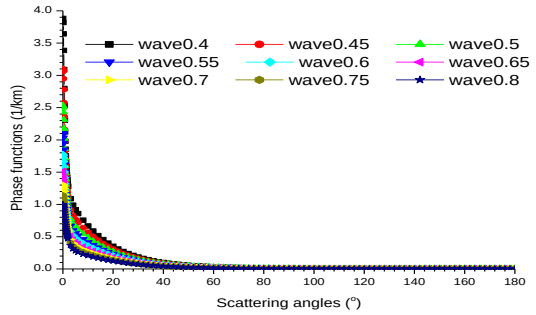

Figure 37(a): A graph of Phase functions against scattering angles at 90% RH SOOT Model 5

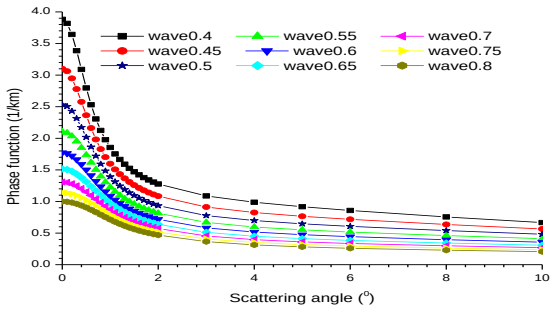

Figure 37(b): A graph of Phase functions against scattering angles at 90% RH SOOT Model 5

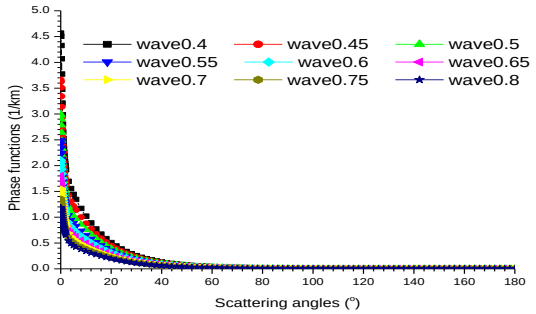

Figure 38(a): A graph of Phase functions against scattering angles at 95% RH SOOT Model 5

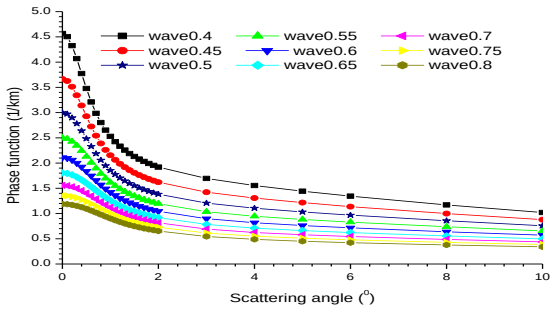

Figure 38(b): A graph of Phase functions against scattering angles at 95% RH SOOT Model 5

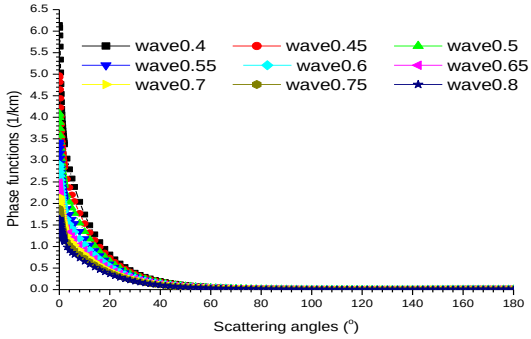

Figure 39(a): A graph of Phase functions against scattering angles at 98% RH SOOT Model 5

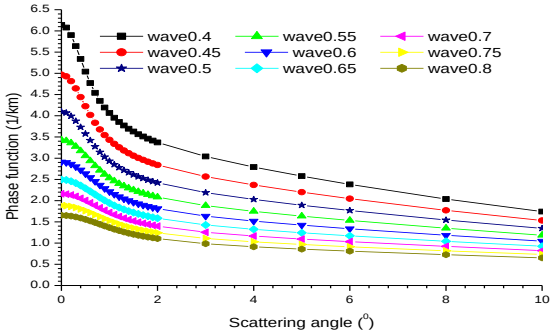

Figure 39(b): A graph of Phase functions against scattering angles at 98% RH SOOT Model 5

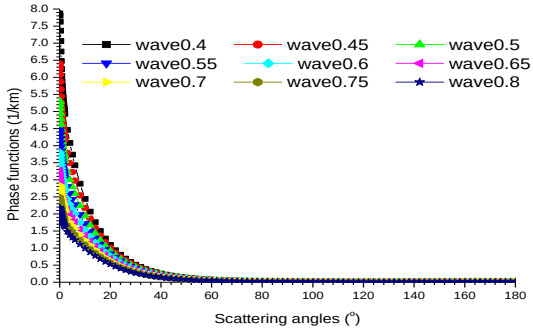

Figure 40(a): A graph of Phase functions against scattering angles at 99% RH SOOT Model 5

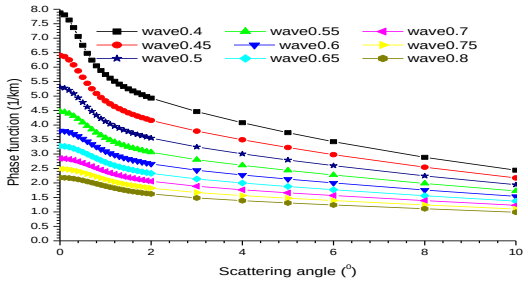

Figure 40(b): A graph of Phase functions against scattering angles at 99% RH SOOT Model 5

Analysis reveals that phase functions exhibit distinct trends in relation to scattering angles, relative humidity, and wavelength. Phase functions decrease with increasing scattering angles, particularly in urban areas with high aerosol concentrations. The phase functions increase with increasing relative humidity due to aerosol growth and enhanced scattering properties. However, phase functions decrease with increasing wavelength, reflecting reduced scattering efficiency. These patterns are consistently observed across Figures 1a-8a and 1b-8b.

The phase functions remaining invariant with respect to increasing soot aerosol concentration due to the dominance of other aerosols and the absorption properties of soot aerosols. The fixed concentrations of water-soluble and water-insoluble aerosols might dominate the phase function, masking the impact of increasing soot aerosol concentration. The soot aerosols are strong absorbers, and their impact on phase functions might be more significant in terms of absorption rather than scattering, limiting their scattering contribution and resulting in minimal changes to the phase function. The increase in soot aerosols contributes to the overall scattering behaviour, the effect of aerosol hydration dominates.

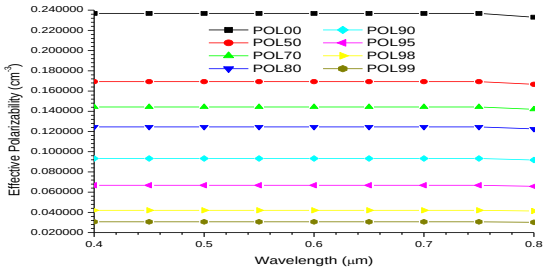

Figure 41: A graph of Effective Polarizability against Wavelength for SOOT Model

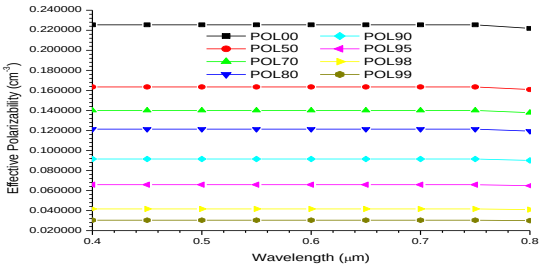

Figure 42: A graph of Effective polarizability against Wavelength for SOOT Model 2

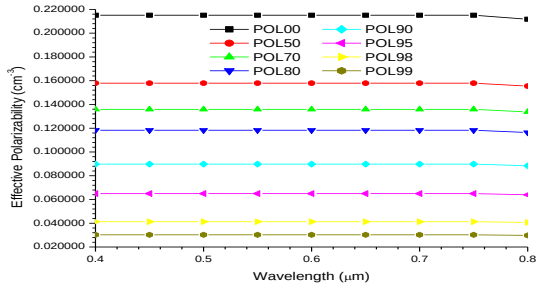

Figure 43: A graph of Effective Polarizability against Wavelength for SOOT Model 3

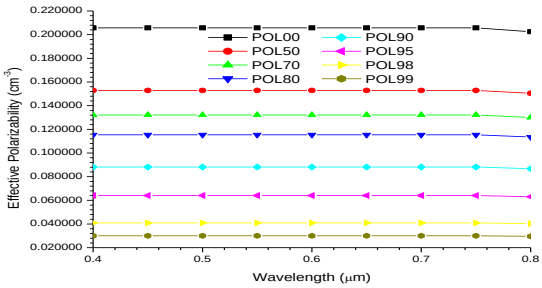

Figure 44: A graph of Effective Polarizability against Wavelength for SOOT Model 4

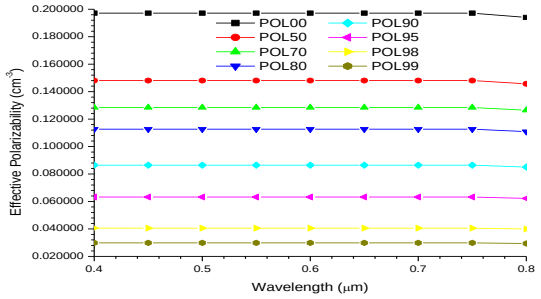

Figure 45: A graph of Effective polarizability against Wavelength for SOOT Model 5

From figure 41 to 45, The effective polarizabilities remain relatively constant with increasing wavelength in urban atmospheres due to the complex refractive index of urban aerosols might not vary significantly with wavelength, leading to relatively constant polarizabilities. The effective polarizabilities decrease with increasing relative humidity due to aerosols in urban atmospheres take up water as relative humidity increases, leading to changes in their optical properties and potentially decreasing polarizabilities. The effective polarizabilities decrease with increasing soot aerosol concentration due to soot aerosols are strong absorbers, and their increasing concentration can lead to a decrease in polarizabilities due to enhanced absorption.

4. Conclusion

This work examined the impact of scattering angles, relative humidity, wavelength, and soot aerosol concentration on phase functions and effective polarizabilities of urban aerosols. Findings indicate that these properties are highly sensitive to the mentioned parameters. Phase functions decrease with increasing scattering angles and wavelength, consistent with previous research (Krekov, 2002; Krekov, 1980). However, phase functions increase with increasing relative humidity due to aerosol hydration and changes in scattering patterns, dominating over the effects of soot aerosols (Hänel, 1998). Phase functions remain relatively invariant with increasing soot aerosol concentration, likely due to the dominance of other aerosols and soot's absorption properties (Bond & Bergstrom, 2006; Andreae & Gelencsér, 2006).

Effective polarizabilities remain relatively constant with increasing wavelength but decrease with increasing relative humidity and soot aerosol concentration, attributed to changes in optical properties and enhanced absorption (Seinfeld & Pandis, 2016; Matin, 2000; Bond *et al.*, 2006).

References

1. Anderson, T. L., R. J. Charlson, S. E. Schwartz, R. Knutti, O. Boucher, H. Rodhe, and J. Heintzenberg (2003). *Climate forcing by aerosols a hazy picture. Science 300*, 1103.
2. Andreae, M. O., & Gelencsér, A. (2006). Black carbon or brown carbon? The nature of light-absorbing carbonaceous aerosols. Atmospheric Chemistry and Physics, 6(10), 3131-3148.
3. Bond, T. C., & Bergstrom, R. W. (2006). Light absorption by carbonaceous particles: An investigative review. Aerosol Science and Technology, 40(1), 27-67.
4. DHänel, G. (1998). Aerosol properties and their influence on climate. Journal of Aerosol Science, 29(Supplement 1), S647-S648.
5. Hess, M., Koepke, P., & Schult, I. (1998). Optical properties of aerosols and clouds: The software package OPAC. *Bulletin of the American Meteorological Society*, 79(5), 831–844. doi: 10.1175/1520-0477(1998)079<0831:OPOAAC>2.0.CO;2
6. Koepke, P., Gaasteiger, J., and Hess, M. (2015). Optical properties of desert aerosol with non-spherical mineral particles: data incorporate to OPAC. Atmospheric Chemistry and Physics, 15, 5947 – 5956. Doi: 10.5194/acp-15-5947-2015
7. Krekov, G. M. (1980). Light scattering by aerosol particles. Journal of Aerosol Science, 11(4), 343-353.
8. Krekov, G. M. (2002). Optical properties of soot aerosol. Journal of Quantitative Spectroscopy and Radiative Transfer, 73(2-5), 287-295

9. Lindqvist H., Jokinen O., Kandler K., Scheuvens D., and Nousiainen T. (2014): Single Scattering by realistic, inhomogeneous mineral dust particles with stereogrammetric shapes. *Atmos. Chem. Phys.*, 14.143-157 doi: 10.5194/acp-14-143-2014.
10. Martin, S. T. (2000). Phase transitions of aqueous atmospheric particles. Chemical Reviews, 100(9), 3403-3454.
11. Mishchenko, M. I., Travis, L. D., & Lacis, A. A. (2002). Scattering, absorption, and emission of light by small particles. Cambridge University Press.
12. Schwartz, S. E. and M. O. Andreae (1996). Uncertainty in climate change caused by aerosols. *Science 272*, 1121-1122.
13. Seinfeld, J. H., & Pandis, S. N. (2016). Atmospheric chemistry and physics: From air pollution to climate change. John Wiley & Sons.
14. Shettle, E. P., and R. W. Fenn, (1979): Models for the aerosols of the lower atmosphere and the effects of humidity variations on their optical properties. *AFGL-TR*-79-0214, 94 pp. [Available from AFCRL, Hanscom Field, Bedford, MA 01731.]
15. Smith, A. B., & Johnson, C. D. (2010). Optical properties of aerosols: A review. *Journal of Atmospheric Sciences*, 67(3), 417–447. doi: 10.1175/2009JAS3087·1